Ceramics-Silikáty 62 (2), 173-180 (2018)
www.ceramics-silikaty.cz doi: 10.13168/cs.2018.0009

STRUCTURE, GLASS STABILITY AND RHEOLOGICAL PROPERTIES OF $Na_2O–CaO–Al_2O_3–SiO_2$ GLASSES DOPED WITH Y_2O_3

YANSHENG HOU*, **, JINSHU CHENG*, ***, #JUNFENG KANG****, JIAN YUAN*, ***, JING CUI**

*State Key Laboratory of Silicate Materials for Architectures, Wuhan University of Technology, Wuhan, 430070, China
**Shaanxi Polytechnic Institute, Xianyang, 712000, China
*** Hebei Shahe Glass Technology Research Institute, Shahe, 054100, China
****School of Materials Science and Engineering, University of Jinan, Jinan, 250000, China

#E-mail: mse_kangjf@ujn.edu.cn

Submitted December 4, 2017; accepted February 16, 2018

Keywords: Structure, Glass stability, Rheological, Fragility, Viscosity

The structure, glass stability and rheological properties of $Na_2O–CaO–Al_2O_3–SiO_2$ glasses with different Y_2O content have been invesigated by DSC, FTIR, rotating crucible viscometer and dilatometry. The results showed that the addition of Y_2O_3 reduced the polymerization degree of glass network, but made the glass structure more compact. The coefficient of thermal expansion, density and glass transition temperature increased with the increase of Y_2O_3 content. The crystallization peak temperature and glass stability decreased firstly and then increased. While the melting temperature and forming temperature showed the opposite trend. The working temperature and Littleton softening point went up gradually. As the Y_2O_3 content changing from 0 to 2 mol. %, the fragility index m decreased firstly and then increased, while the glasses working temperature range ΔT experienced an opposite change.

INTRODUCTION

Aluminosilicate glasses doped with rare-earth elements have attracted large attentions because of their interesting physical and chemical properties, such like high glass transition temperature T_g [1, 2], high hardness and elastic modulus [3], excellent chemical [4, 5] and thermal resistance [6], or high refractive index [7]. Therefore, these glasses have been widely used for optical communications, laser technology and other fields [2, 8]. These excellent properties are closely related to their special structure characteristics. The structural role of ions in aluminosilicate glasses is determined by their ionic radius and charge [9]. The ionic radius controls their coordination number in the glass structure. With the radius of the rare earth ions decreasing, the coordination number undergoes a shift from 7 or 8 to 6 [10]. Generally, rare earth ions are assumed to act as network modifiers, which are isolated between $[SiO_4]$ and $[AlO_4]$ tetrahedra [11]. However, their cationic field strengths (CFS = Z/r^2, where Z is the charge of the element and r its ionic radius) are much higher than more common network modifier cations (e.g. Na^+, K^+ and Ca^{2+}), which are considered to fall at the low end of "intermediate" cations [8].

At present, the fundamental and application research of rare earth doped aluminosilicate glasses on their physical and chemical properties has been widely conducted. However, to our best knowledge, there are very little available data for the effect of rare earth on the viscosity and rheological properties of the aluminosilicate glass melts. And these properties are very important for glass melting, fining, processing optimization, and annealing process [12, 13]. In addition, glass forming ability (GFA) is also an important parameter for glass production process, which determines the easiness to vitrify a melt on cooling process [14]. However, it is quite difficult to accurately measure [15]. Therefore, many researchers proposed that glass stability (GS) against devitrification on heating can be used to estimate GFA [15-18]. Generally, GS is easily derived from characteristic temperatures that are determined from DTA or DSC analyses.

In this work, the density, coefficient of thermal expansion and glass stability of $Na_2O–CaO–Al_2O_3–SiO_2$ glasses doped with Y_2O_3 were investigated. FTIR analysis was used to elucidate the relationship between structure and these properties. At last, the effect of Y_2O_3 content variation on the rheological properties of $Na_2O–CaO–Al_2O_3–SiO_2$ glass at high temperatures was investigated.

EXPERIMENTAL

$Na_2O–CaO–Al_2O_3–SiO_2$ glasses doped with different content of Y_2O_3 were synthesized and investigated in this work. The starting materials SiO_2, Na_2CO_3, $CaCO_3$, Al_2O_3 and Y_2O_3 were all analytical chemicals, and their purity was more than 99 % (wt. %). The chemical

compositions of these glass samples (mol. %) are listed in Table 1. The glass samples with 0, 0.5 1.0, 1.5 and 2 mol. % Y_2O_3 were labeled as Y0, Y1, Y2, Y3 and Y4, respectively. Glass batches were mixed thoroughly, and then melted in alumina crucibles at 1510~1530°C for 2 h. The part of melts were poured onto a pre-heated stainless steel mold to form, and then annealed at 50°C below their glass transition temperature T_g for 2 h . The residual melts were poured into cold water and dried at 120°C for 24 h to obtain glass frits for viscosity tests.

Table 1. Chemical compositions of the glass samples with different Y_2O_3 content (mol. %).

No.	Na_2O	CaO	Al_2O_3	SiO_2	Y_2O_3
Y0	14.73	11.65	12.79	60.88	0
Y1	14.73	11.65	12.79	60.88	0.5
Y2	14.73	11.65	12.79	60.88	1.0
Y3	14.73	11.65	12.79	60.88	1.5
Y4	14.73	11.65	12.79	60.88	2.0

The dilatometric measurements were performed in a horizontal dual-rod dilatometer (Model DIL 402, Netzsch, Germany) at a heating rate of 5°C·min^{-1}. The dilatometric softening temperature T_d and coefficient of thermal expansion (CTE, $\alpha_{25-300°C}$) of glasses were determined. Regular bulk glass sticks with the dimension 4 mm × 4 mm × 25.4 mm were prepared for dilatometry. The density ρ was measured by Archimedes'principle with deionized water as the immersion solution. And the average value was obtained from the five test results of every glass sample to reduce the errors.

To determine the glass transition temperature T_g, crystallization temperature T_c and liquidus temperature T_l, the monolithic samples of each glass (4 × 4 × 1 mm) were measured by DSC method (Netzsch STA 409, German) in air atmosphere at the heating rate of 10°C min^{-1} from 20 to 1200°C respectively, using Al_2O_3 as reference material. The platinum crucible was used in the DSC tests. Air flow rate through the sample pan was kept constant at 50 ml·min^{-1}.

The viscosities of the glass melts in the high temperature range were tested by the rotating crucible viscometer (Model Rheotronic II). About 200 g glass frits for each sample were added into a platinum crucible and placed into the furnace set at 1500°C.

The structure of glasses were measured with Infrared spectrometer (Nico-let-380). The KBr pressing method was used in this work. About 1 mg glass sample and 0.1 g KBr were mixed throughly by grinding. A sample of tablets with a diameter of 10 mm and a thickness of 1mm was prepared with mixed powders and was analyzed. The FTIR spectrum was recorded at the range of wave numbers from 400 to 1400 cm^{-1}.

RESULTS AND DISCUSSION

Structure

FTIR absorption spectral curves of annealed glass samples with different Y_2O_3 content are illustrated in Figure 1. There were three main absorption bands in the 400 - 1400 cm^{-1} region. Absorption bands of glasses and their assignments were listed in Table 2. The bands at 400 - 500 cm^{-1} is due to the bending vibrations of Si–O–Si and Si–O–Al linkages [19, 20]. The absorption bands in the 650 - 800 cm^{-1} is considered as Al–O stretching vibration of [AlO_4] tetrahedron [20, 21]. The broad bands in the 800 - 1300 cm^{-1} is assigned to anti-symmetric stretching modes of the Si–O–Si bonds of the Q^n units (n means the number of bridging oxygens within a tetrahedron, n = 0, 1, 2, 3 and 4) [1, 22, 23]. With n value increasing from 0 to 4, the absorption bands of the Q^n units were centered around 850, 900, 950, 1100 and 1200 cm^{-1}, respectively [1, 20].

Figure 1 showed that the presence of Y_2O_3 in Na_2O–CaO–Al_2O_3–SiO_2 glasses had little influence on the peaks at about 466 and 730 cm^{-1}. Comparing with the base glass, the Y_2O_3 content increasing lead to the peak at around 1036 cm^{-1} shift to lower wavenumbers and the

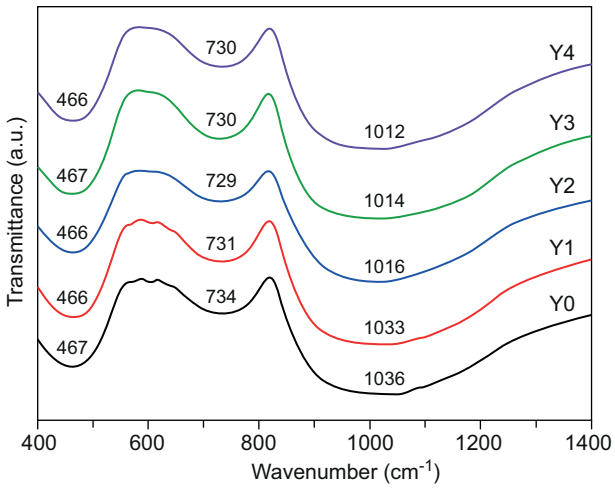

Figure 1. FTIR absorption spectral curves of annealed glass samples.

Table 2. Absorption bands of glasses and their assignments.

Peak position	Assignment	References
400 - 500 cm^{-1}	Bending vibrations of Si–O–Si and Si–O–Al linkages	[19, 20]
650 - 800 cm^{-1}	Al–O stretching vibration of [AlO_4] units	[20, 21]
800 - 1300 cm^{-1}	Si–O–Si asymmetric stretching of [SiO_4] units	[1, 22, 23]

absorption band at 800 - 1300 cm^{-1} become broader. The main absorption band was centered at ~1036 cm^{-1}, which indicated a distribution of Q^n units centered between the Q^2 and Q^3 units. While the broadening of this absorption band toward lower wave numbers indicated the network structure depolymerized. It suggested that Y^{3+} ions acted as network modifiers and increased the number of NBO (non-bridging oxygen) in the glasses.

The change of Si–O bond strength in soda lime aluminosilicate glasses doped Y_2O_3 can be assessed with the equation $F_{Si-O} = 4\pi^2 c^2 \mu \nu^2$, where c is the speed of light, μ the reduced mass of cation, and ν the peak frequency [21]. It has been observed that the peak frequency in the 800 - 1300 cm^{-1} decreased from 1036 to 1012 cm^{-1}, and consequently caused the Si–O bond strength to decrease as the doping content of Y_2O_3 increase from 0 to 2 mol. %. Furthermore, it also can be assumed that the larger polarizing force of Y^{3+} ion elongated the Si-O bond length, which caused the Si-O bond strength to become weaker.

Physical properties (CTE and density)

Figure 2 illustrates coefficient of thermal expansion for glass samples with different Y_2O_3 content. With the increase of Y_2O_3 content, the coefficient of thermal expansion (25 – 300°C) of glass samples showed a slight increase from 93.8 to 95.8 × 10^{-7} °C.

The asymmetry of the amplitude of thermal vibrations in the glass determines the thermal expansion, which decreases as the rigidity of glass network increases [13]. The increase of nonbridging oxygen (NBO) will strengthen the asymmetry of the bond to the neighbouring network former cations, which leads to an increase in thermal expansion coefficient. According to the FTIR results, Y^{3+} ions serve as glass network modifiers rather than as network formers in these glasses. The introduction of Y^{3+} ions increase the numbers of NBOs and the Si–O bond length [6]. Thus, the addition of Y^{3+} ions lead to the increase of CTE.

The density of glass samples with different rare earth oxide content is shown in Figure 3. It was able to observe that the density of glasses increased gradually from 2.56 to 2.61 g·cm^{-3} with the Y_2O_3 content increasing.

The molecular mass of Y_2O_3 (225.81 g·mol^{-1}) is markedly higher than that of the other oxides, which is the dominant factor affecting the change in density for all glass samples [24]. The density is an essential macroscopic parameter to characterize the structure of glass. As network modifiers, rare earth metal ions filled space in glass network [25]. Y^{3+} ions possess smaller radius, high filed strength and large coordination number, which attract the neighbor anion groups and make the glass structure more compact as the degree of polymerization reduces. Therefore, the density increased with the Y_2O_3 content increasing.

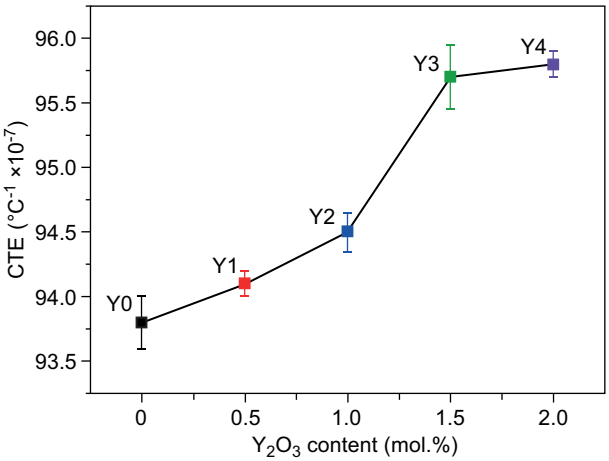

Figure 2. Coefficient of thermal expansion for glass samples with different Y_2O_3 content.

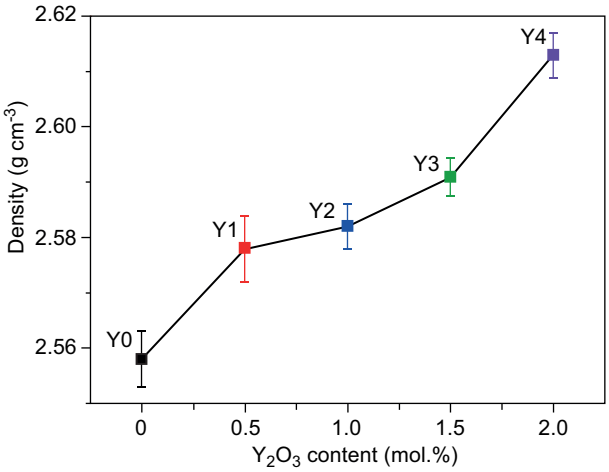

Figure 3. The density of glass samples doped with different Y_2O_3 content.

Stability of the glasses

The results of thermal properties for the glasses investigated by DSC are shown in Figure 4. And glass transition temperature (T_g), crystallization peak temperature (T_c), liquidus temperature (T_l), and the value of K_H for Y0-Y4 are shown in Table 3. The results showed that the glass transition temperature T_g of the samples gradually increased with Y_2O_3 content increasing. The crystallization peak became sharp, then gradually

Table 3. Glass transition temperature (T_g), crystallization peak temperature (T_c), liquidus temperature (T_l), and the value of K_H for Y0-Y4.

No.	T_g (°C)	T_c (°C)	T_l (°C)	K_H
Y0	655	993	1167	1.94
Y1	656	972	1166	1.63
Y2	661	943	1165	1.27
Y3	663	988	1166	1.83
Y4	665	991	1165	1.87

flattened, and its values decreased firstly and then increased, which indicated that a small amount of Y_2O_3 promoted the crystallization of the glasses. When Y_2O_3 content exceeded 1 mol. %, crystallization process was inhibited. The changes of Y_2O_3 content had little effect on the liquidus temperature T_l, which fixed at about 1166°C. The term glass stability refers to the ability of a glass to resist crystallization upon heating. Generally, the glass stability can be evaluated from the correlation among the characteristic temperatures such as T_g, T_c and T_l. One of the glass stability index is the Hrubÿ parameter (K_H) [26]:

$$K_H = \frac{T_c - T_g}{T_l - T_c} \quad (1)$$

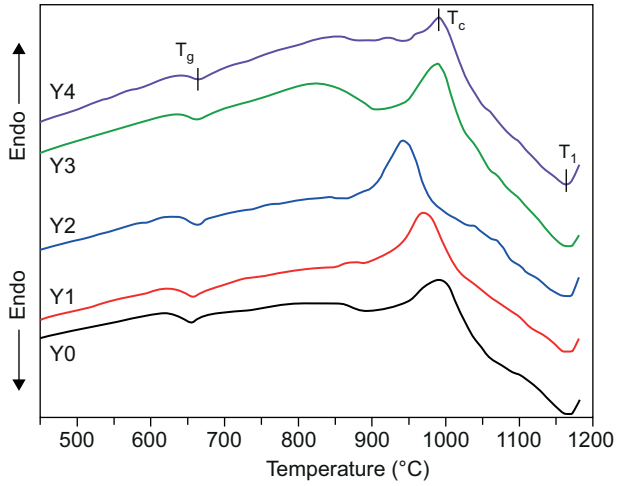

Figure 4. The DSC curves of glass samples with different Y_2O_3 content at 10°C·min^{-1}.

The larger the parameter K_H, the higher is the glass stability. Since an inverse linear relation is found between K_H and the critical cooling rate, K_H may be used as a measure of glass forming ability (GFA) of a melt upon cooling [16, 17]. Table 3 showed that the K_H value decreased firstly and then increased, and reached the minimum value at Y_2O_3 = 1 mol. %. This result indicated that the critical cooling rate of Y2 was hightest, and its glass forming ability was worst.

The role played by a cation in a glass may be classified as network former, intermediate and modifier by simple general criteria based upon bond energies and ionic field strength [27-29]. Rare earth ions are expected to have a modifier character. The proposed structure of the local network of the glasses doped with Y_2O_3 was showed in Figure 5. As network modifier, Y_2O_3 will lead to a depolymerization of glass network, which caused the non-bridging oxygen increasing. However, Y^{3+} ion is very different from Ca^{2+} and Na^+ ions [8]. As trivalent ion, Y^{3+} ion can connect three non-bridging oxygens at the same time, which can link different network structure units (Q^n). For network modifier ions, strength of the connection ≡Si–O–M–O–Si≡ depends largely on the cationic field strength CFS. The greater the CFS, the greater the aggregation effect. Compared with Na^+ and Ca^{2+} ions, Y^{3+} has the largest field strength and the most obvious agglomeration effect (shown as in Table 4). The polymerization extent of glass network decreased, but the network become more compact with Y_2O_3 content increasing. This is in good agreement with the change of glass density and glass transition temperature.

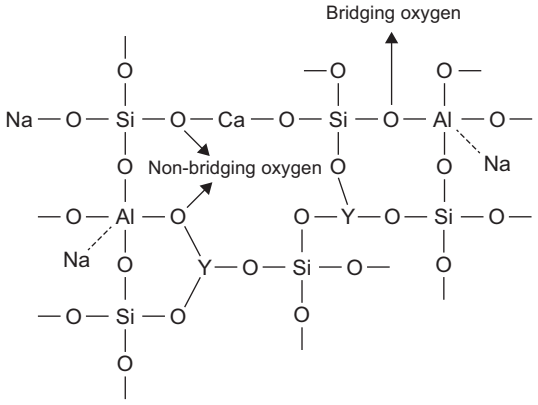

Figure 5. Proposed structure of the local network of the glasses doped with Y_2O_3.

Table 4. Various parameters of Na^+, Ca^{2+} and Y^{3+} ions.

No.	Valence	Ionic radius (Å)	Cationic field strength (Å^{-2})
Na	1	1.16 [30]	0.74
Ca	2	0.99 [31]	2.04
Y	3	0.89 [32]	3.79

Rheological properties of the melts

From glass transition temperature to the glass melting temperature, the viscosity spans more than 12 orders of magnitude. In order to describe the relationship between viscosity and temperature for silicate melts, various models, such like Arrhenius equation, Vogele-Fulchere-Tamman (VFT) equation, Adame Gibbs equation and Mauro–Yue–Ellison–Gupta–Allan (MYEGA) equation, are commonly used for fitting and describing the temperature dependence of viscosity [6, 12, 33, 34]. Among them, the MYEGA equation is more precisely to describe the temperature dependence of viscosity in the long temperature range, as shown below [34]:

$$\log_{10}\eta(T) = \log_{10}\eta_\infty + \frac{K}{T}\exp\left(\frac{C}{T}\right) \quad (2)$$

where η_∞ is the high-temperature limit of the liquid viscosity, and K and C are constants. The high viscosity data (in Pa·s) were obtained directly from the rotating

crucible viscometer. While the T_g measured by DSC (Table 2) and T_d measured by dilatometry can stand for the low viscosity data of $10^{12.4}$ Pa·s and 10^{10} Pa·s respectively [35]. The viscosities of glass samples between the range of glass melting temperature and transition temperature were well fitted by the Equation 2. Taking Y0 as an example, the fitting result is showed in Figure 6. The temperatures at the viscosities of 10, 10^2, 10^3 and $10^{6.6}$ Pa·s are referred to the melting temperature (T_m), forming temperature, working temperature and Littleton softening point, respectively [30, 35]. The constants η_∞, K and C of the Equation 2 and some characteristic temperature points in glass technology were calculated and listed in Table 5. Figure 7 shows the characteristic temperature points of the glass melts with different Y_2O_3 content. It was obvious that melting temperature (T_m) and forming temperatures increased firstly and then decreased with Y_2O_3 content increasing, which both peaked at 1 mol. % Y_2O_3. While the working temperature increased firstly, and then maintained stable at about 1081°C. The inflection point also appeared at 1 mol. % Y_2O_3. The Littleton softening point monotonically increased with Y_2O_3 content increasing.

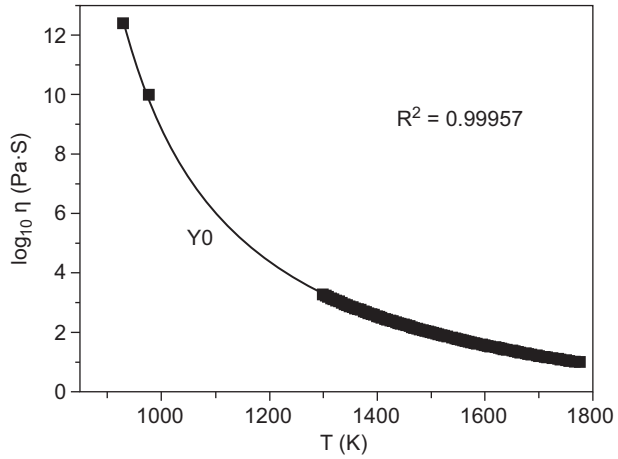

Figure 6. Viscosity as a function of temperature for glass sample Y0. The solid lines represented fitting curves obtained by Equation 2.

The results indicated that both temperature and content have a large effect on the roles played by Y_2O_3 in glass network. When Y_2O_3 content ≤ 1 mol. %, Y^{3+} ions mainly play the role of agglomeration in both high temperature and low temperature ranges, which compacted the glass structure and increased the viscosity of glass metls. When Y_2O_3 content is greater than 1 mol. %, Y_2O_3 showed different effects on viscosity at high temperature and low temperature. Between the melting and forming temperature ranges, a large amount of Y_2O_3 brought more free oxygens, which reacted with bridging oxygens to create a lot of non-bridging oxygens. This leads to loosening of the glass network structure and decreasing viscosity of the melts, resulting in a decrease of melting temperature (T_m) and forming temperature. For the working temperature, the effects of agglomeration and depolymerization on viscosity are offset, resulting in the viscosity stabilizing at a certain value. With the further reduction of temperature, agglomeration plays a major role. Therefore, the Littleton softening point monotonically increased with Y_2O_3 content increasing. This also caused T_g and T_d going up with Y_2O_3 content increasing.

The temperature interval (ΔT) between the working point and Littleton softening point was used to estimate the workability of the glass melt [35, 36]. Table 5 showed that the temperature intervals corresponding to the workability became wider firstly and then shorter with the Y_2O_3 content increasing.

The temperature dependence of the viscosity for various glass forming materials can be characterized by Angell's plot [37]. By plotting the logarithm of the viscosity as a function of the reduced inverse temperature T_g/T, curves with different degrees of non-Arrhenius behavior may be systematized. The degree of deviation from the Arrhenius behavior is called fragility [38]. In addition molten SiO_2 is known as the strongest liquid [39]. The logarithmic viscosity ($\log_{10}\eta$) of Y0 has been plotted as a function of the inverse temperature scaled by T_g/T (Figure 8). Fragility is defined as the slope of the $\log_{10}\eta$ versus T_g/T curve at T_g, shown as Equation 3:

$$m = \frac{\partial(\log_{10}\eta)}{\partial(T_g/T)}\Big|_{T=T_g} \quad (3)$$

Table 5. Parameters for the Equation 2 and characteristic temperatures of forming process for glass samples.

Sample	Y0	Y1	Y2	Y3	Y4
η_∞	-0.58	-0.65	-0.69	-0.70	-0.72
K	606.20	650.70	677.79	661.45	663.85
C	2772.66	2720.56	2704.59	2737.57	2744.51
m	51.76	51.26	50.98	51.41	51.50
Melting point (°C)	1522	1524	1529	1518	1516
Forming point (°C)	1223	1228	1238	1234	1234
Working point (°C)	1067	1073	1081	1081	1081
Littleton softening point (°C)	813	816	823	825	827
Workability ΔT (°C)	254	257	258	256	254

With the definition, Equation 2 can be rewritten, shown as Equation 4. Then the fragility index *m* can be obtained by fitting the viscosity data with Equation 4.

$$\log_{10}\eta\,(T) = \log_{10}\eta_\infty + (12.4 - \log_{10}\eta_\infty)\,\frac{T_g}{T}\exp\left[\left(\frac{m}{12.4-\log_{10}\eta_\infty} - 1\right)\left(\frac{T_g}{T} - 1\right)\right] \quad (4)$$

The the values of fragility index *m* for diefferent glass samples are showed in Table 5. The results showed that the strongest liquid of the glass investigated in this paper was sample Y2, while the most fragile one was sample Y0. It was obviously that there was an inverse correlation between the workability and fragility index *m*, shown as Figure 9. As the Y_2O_3 content increasing from 0 to 2 mol. %, the fragility index *m* decreased firstly and then increased, while workability ΔT experienced an opposite changes, which is consistent with the results from other researchers [12, 35, 36].

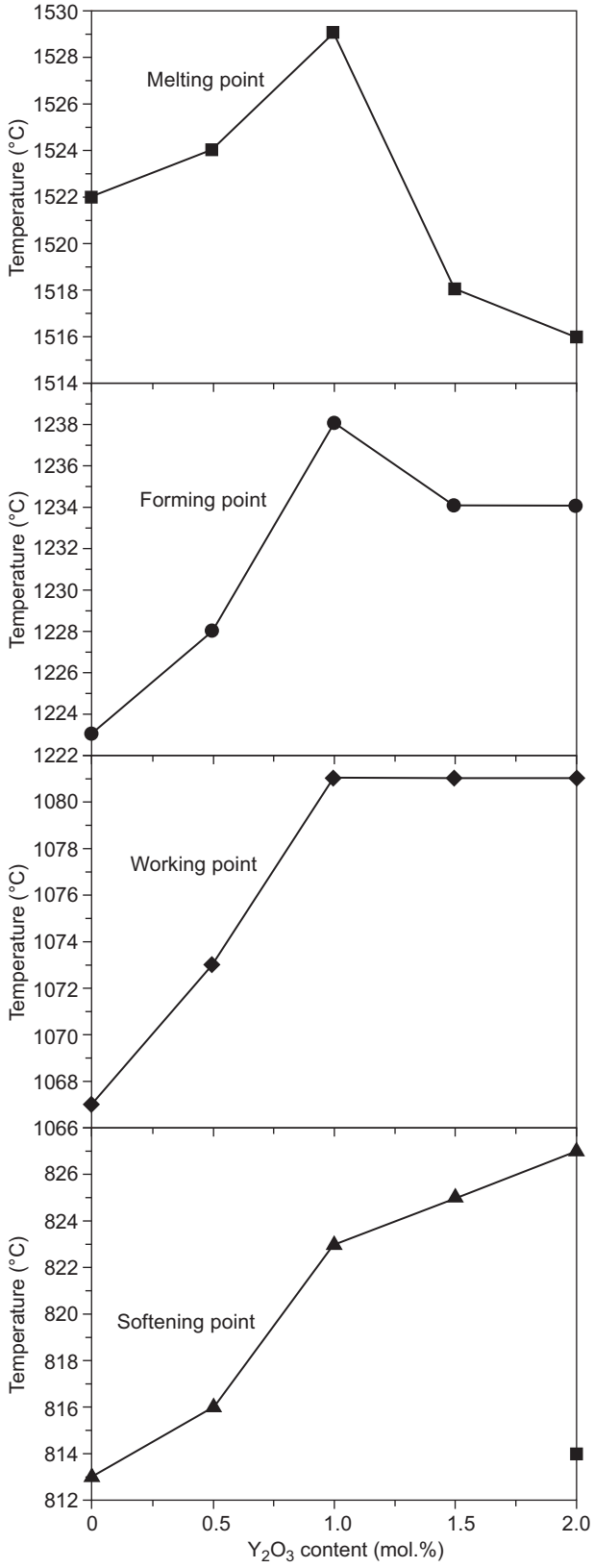

Figure 7. Characteristic temperature points of the glass melts with different Y_2O_3 content.

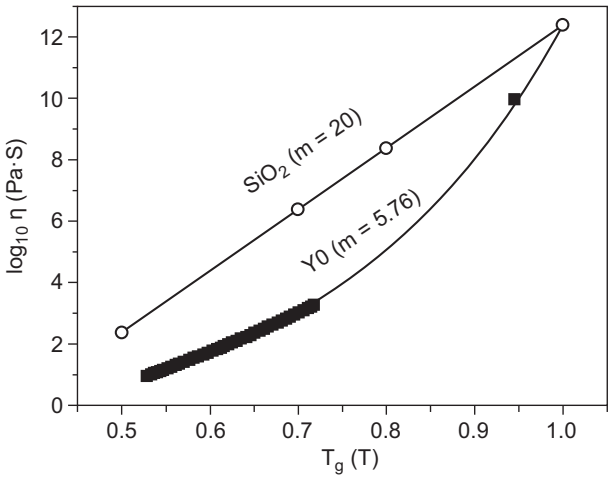

Figure 8. The logarithmic viscosity ($\log_{10}\eta$) of the inverse temperature scaled by T_g as a function T_g/T.

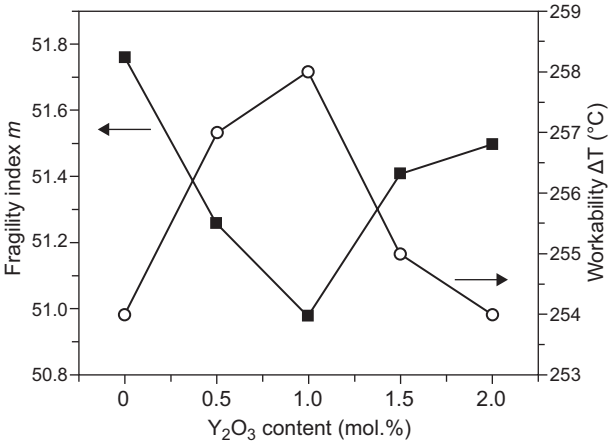

Figure 9. The fragility index m and workability ΔT of the glass samples with different Y_2O_3 content.

CONCLUSIONS

With the increase of Y_2O_3 content, the glass network polymerization extent decreased, but the structure became more compact. The coefficient of thermal expansion and density increased from 93.8 to 95.8 × 10^{-7} °C and 2.56 to 2.61 g·cm^{-3}, respectively. The glass transition temperature increased monotonously, while the crystallization peak temperature and glass stability decreased firstly and then increased. It was obvious that melting temperature (T_m) and forming temperatures increased firstly and then decreased, while working temperature and Littleton softening point increased with Y_2O_3 content increasing. As the Y_2O_3 content increasing from 0 to 2 mol. %, the fragility index *m* decreased firstly and then increased, while the glasses working temperature range ΔT experienced an opposite change. All inflection points of different properties in this paper appeared at Y_2O_3 = 1 mol. %.

Acknowledgements

This work was funded by the National Key Research and Development Program of China (No. 2016YFB0303702)

REFERENCES

1. Aronne A., Esposito S., Pernice P. (1997): FTIR and DTA study of lanthanum aluminosilicate glasses. *Materials Chemistry and Physics*, *51* (2), 163–168. doi: 10.1016/S0254-0584(97)80287-8
2. Florian P., Sadiki N., Massiot D., Coutures J.P. (2007): ^{27}Al NMR study of the structure of lanthanum- and yttrium-based aluminosilicate glasses and melts. *Journal of Physical Chemistry B*, *111* (33), 9747-9757. doi: 10.1021/jp072061q
3. Johnson J., Weber R., Grimsditch M. (2005): Thermal and mechanical properties of rare earth aluminate and low-silica aluminosilicate optical glasses. *Journal of Non-Crystalline Solids*, *351* (8–9), 650-655. doi:10.1016/j.jnoncrysol.2005.01.065
4. Bois L., Barr, Eacute N., Guittet M.J., Guillop, Eacute S., Trocellier P., Gautier-Soyer M., Verdier P., Laurent Y. (2002): Aqueous corrosion of lanthanum aluminosilicate glasses: influence of inorganic anions. *Journal of Nuclear Materials*, *300* (2), 141-150. doi: 10.1016/S0022-3115(01)00748-6
5. Bois L., Guittet M.J., Barré N., Trocellier P., Guillopé S., Gautier M., Verdier P., Laurent Y. (2000): Aqueous alteration of lanthanum alumino-silicate glasses. *Journal of Non-Crystalline Solids*, *276* (1), 181-194. doi: 10.1016/S0022-3093(00)00275-1
6. Wang M.T., Cheng J.S., Li M., He F., Deng W. (2012): Viscosity and thermal expansion of soda-lime-silica glass doped with Gd_2O_3 and Y_2O_3. *Solid State Sciences*, *14* (8), 1233-1237. doi: 10.1016/j.solidstatesciences.2012.06.001
7. Singh S., Kalia G., Singh K. (2015): Effect of intermediate oxide (Y_2O_3) on thermal, structural and optical properties of lithium borosilicate glasses. *Journal of Molecular Structure*, *1086*, 239-245. doi: 10.1016/j.molstruc.2015.01.031
8. Schaller T., Stebbins J.F. (1998): The Structural Role of Lanthanum and Yttrium in Aluminosilicate Glasses: A ^{27}Al and ^{17}O MAS NMR Study. *Journal of Physical Chemistry B*, *102* (11), 10690-10697. doi: 10.1002/chin.199911014
9. Marchi J., Morais D.S., Schneider J., Bressiani J.C., Bressiani A.H.A. (2005): Characterization of rare earth aluminosilicate glasses. *Journal of Non-Crystalline Solids*, *351* (10), 863-868. doi: 10.1016/j.jnoncrysol.2005.01.078
10. Wang J., Brocklesby W.S., Lincoln J.R., Townsend J.E., Payne D.N. (1993): Local structures of rare-earth ions in glasses: the 'crystal-chemistry' approach. *Journal of Non-Crystalline Solids*, *163* (3), 261-267. doi: 10.1016/0022-3093(93)91303-K
11. Wang J., Liu C., Zhang G., Xie J., Li N., Han J., Zhao X. (2016): Thermal expansion and crystallization behaviour of magnesium aluminosilicate glasses doped with neodymium ions. *Physics and Chemistry of Glasses – European Journal of Glass Science and Technology Part B*, *57* (3). doi: 10.13036/17533562.57.3.081
12. Kang J., Wang J., Cheng J. (2017): Structure and properties of $CaO–MgO–Al_2O_3–SiO_2$ glasses obtained by vitrification of granite wastes. *Physics and Chemistry of Glasses: European Journal of Glass Science and Technology Part B*, *58* (6), 249-255. doi: 10.13036/17533562.58.6.033
13. Wang M.T., Cheng J.S. (2010): Viscosity and Thermal Expansion of Rare Earth Containing Soda-Lime-Silicate Glass. *Journal of Alloys and Compounds*, *504* (1), 273-276. doi: 10.1016/j.jallcom. 2010.05.111
14. Kohara S., Akola J., Morita H., Suzuya K., Weber J.K., Wilding M.C., Benmore C.J. (2011): Relationship between topological order and glass forming ability in densely packed enstatite and forsterite composition glasses. *Proceedings of the National Academy of Sciences of the United States of America*, *108* (36), 14780. doi:10.1073/pnas.1104692108/-/DCSupplemental
15. Nascimento M.L.F., Souza L.A., Ferreira E.B., Zanotto E.D. (2005): Can glass stability parameters infer glass forming ability? *Journal of Non-Crystalline Solids*, *351* (40–42), 3296-3308. doi: 10.1016/j.jnoncrysol.2005.08.013
16. Marques T.V.R., Cabral A.A. (2014): Influence of the heating rates on the correlation between glass-forming ability (GFA) and glass stability (GS) parameters. *Journal of Non-Crystalline Solids*, *390* (8), 70-76. doi: 10.1016/j.jnoncrysol.2014.02.019
17. Kozmidis-Petrovic A., Šesták J. (2012): Forty years of the Hrubý glass-forming coefficient via DTA when comparing other criteria in relation to the glass stability and vitrification ability. *Journal of Thermal Analysis and Calorimetry*, *110* (2), 997-1004. doi: 10.1007/s10973-011-1926-6
18. Cabral A.A., Cardoso A., Zanotto E.D. (2002): Glass-forming ability versus stability of silicate glasses. *Journal of Non-Crystalline Solids*, *2003* (320), 1-8. doi:10.1016/S0022-3093(03)00079-6
19. Shimizu F., Tokunaga H., Saito N., Nakashima K. (2006): Viscosity and Surface Tension Measurements of RE_2O_3-MgO-SiO_2 (RE=Y, Gd, Nd and La) Melts. *ISIJ International*, *46* (3), 388-393. doi: 10.2355/isijinternational.46.388
20. Clayden N.J., Esposito S., Aronne A., Pernice P. (1999): Solid State ^{27}Al NMR and FTIR Study of Lanthanum Aluminosilicate Glasses. *Journal of Non-Crystalline Solids*, *258* (1), 11-19. doi: 10.1016/S0022-3093(99)00555-4

21. Hou Y., Yuan J., Kang J., Cui J., Cheng J., Cui J. (2017): Effects of rare earth oxides on viscosity, thermal expansion, and structure of alkali-free boro-aluminosilicate glass. *Journal of Wuhan University of Technology-Mater. Sci. Ed.*, *32* (1), 58-62. doi: 10.1007/s11595-017-1558-1
22. Zeng H., Yang Y., Lin Z., Liang X., Yuan S., Chen G., Sun L. (2011): The Effect of B_2O_3 on the Luminescent Properties of Eu Ion-Doped Aluminoborosilicate Glasses. *Journal of Non-Crystalline Solids*, *357* (11), 2328-2331. doi:10.1016/j.jnoncrysol.2010.11.093
23. Wang M.T., Li M., Cheng J.S., He F. (2014): Structure and Viscosity of Soda Lime Silicate Glasses with Varying Gd_2O_3 Content. *Journal of Molecular Structure*, *1063* (16), 139-144. doi: 10.1016/j.molstruc.2014.01.062
24. Mansour E. (2012): Semi-quantitative analysis for FTIR spectra of Al_2O_3–PbO–B_2O_3–SiO_2 glasses. *Journal of Non-Crystalline Solids*, 3*58* (3), 454-460. doi:10.1016/j.jnoncrysol.2011.10.037
25. Lu Y., Liu H., Qu Y., Lu H., Huang S., Yue Y. (2017): Influence of La_2O_3 and Ce_2O_3 additions on structure and properties of aluminoborosilicate glasses. *Journal of Materials Science Materials in Electronics*, *28* (3), 2716-2722. doi: 10.1007/s10854-016-5850-1
26. Hrubý A. (1972): Evaluation of Glass Forming Tendency by Means of DTA. *Czechoslovak Journal of Physics B*, *22* (11), 1187-1193. doi: 10.1007/BF01690134
27. Liu S., Kong Y., Tao H., Sang Y. (2016): Crystallization of a highly viscous multicomponent silicate glass: Rigidity percolation and evidence of structural heterogeneity. *Journal of the European Ceramic Society, 37(2), 715-720*. doi: 10.1016/j.jeurceramsoc.2016.08.038
28. Han X., Tao H., Gong L., Wang X., Zhao X., Yue Y. (2014): Origin of the frequency shift of Raman scattering in chalcogenide glasses. *Journal of Non-Crystalline Solids*, *391* (3), 117-119. doi: 10.1016/j.jnoncrysol.2014.03.021
29. Tao H., Zhao X., Liu Q. (2013): Optical non-linearity in nano- and micro-crystallized glasses. *Journal of Non-Crystalline Solids*, *377* (10), 146-150. doi: 10.1016/j.jnoncrysol.2013.02.001
30. Zheng W.H., Cao H., Zhong J.B. (2015): CaO–MgO–Al_2O_3–SiO_2 glass-ceramics from lithium porcelain clay tailings for new building materials. *Journal of Non-Crystalline Solids*, 4*05*, 27-33. doi: 10.1016/j.jnoncrysol.2014.11.002
31. Raghavaiah B.V., Rao R.B., Veeraiah N., Babu P., Jayasankar C.K. (2004): Spectroscopic properties of MO–WO_3–P_2O_5: Ho^{3+} glasses. *The European Physical Journal – Applied Physics*, *26* (3), 169-176. doi: 10.1051/epjap:2004035
32. Wang X., Yan X., Kan C. (2011): Controlled synthesis and optical characterization of multifunctional ordered Y_2O_3:Er^{3+} porous pyramid arrays. *Journal of Materials Chemistry*, *21* (12), 4251-4256. doi: 10.1039/c0jm03761c
33. Zheng Q., Mauro J.C. (2016): Viscosity of glass-forming systems. *Journal of the American Ceramic Society*, *100* (1), 6-25. doi: 10.1111/jace.14678
34. Mauro J.C., Yue Y.Z., Ellison A.J., Gupta P.K., Allan D.C. (2009): Viscosity of Glass-Forming Liquids. *Proceedings of the National Academy of Sciences*, *106* (47), 19780-19784. doi: 10.1073 pnas. 0911705106
35. Cheng J.S., Xiao Z.F., Yang K., Wu H. (2013): Viscosity, fragility and structure of Na_2O–CaO–Al_2O_3–SiO_2 glasses of increasing Al/Si ratio. *Ceramics International*, *39* (4), 4055-4062. doi: 10.1016/j.ceramint.2012.10.258
36. Wang M.T., Fang L., Li M., Cheng J.S., He F., Deng W., Dongol R. (2016): Dependence of Gd_2O_3 containing silicate glass workability and fragility on structure. *Materials Chemistry and Physics*, *179*, 304-309. doi: 10.1016/j.matchemphys.2016.05.043
37. Angell C.A. (1995): Formation of Glasses from Liquids and Biopolymers. *Science*, *267* (5206), 1924-1935. doi: 10.1126/science.267.5206.1924
38. Angell C.A. (1991): Relaxation in liquids, polymers and plastic crystals – strong/fragile patterns and problems *Journal of Non-Crystalline Solids*, s 131–133 (6), 13-31. doi: 10.1016/0022-3093(91)90266-9
39. Shan Z., Li C., Tao H. (2017): Mixed alkaline earth effect on the mechanical and rheological properties of Ca–Mg silicate glasses. *Journal of the American Ceramic Society*, *100,*4570–4580. doi: 10.1111/jace.14999